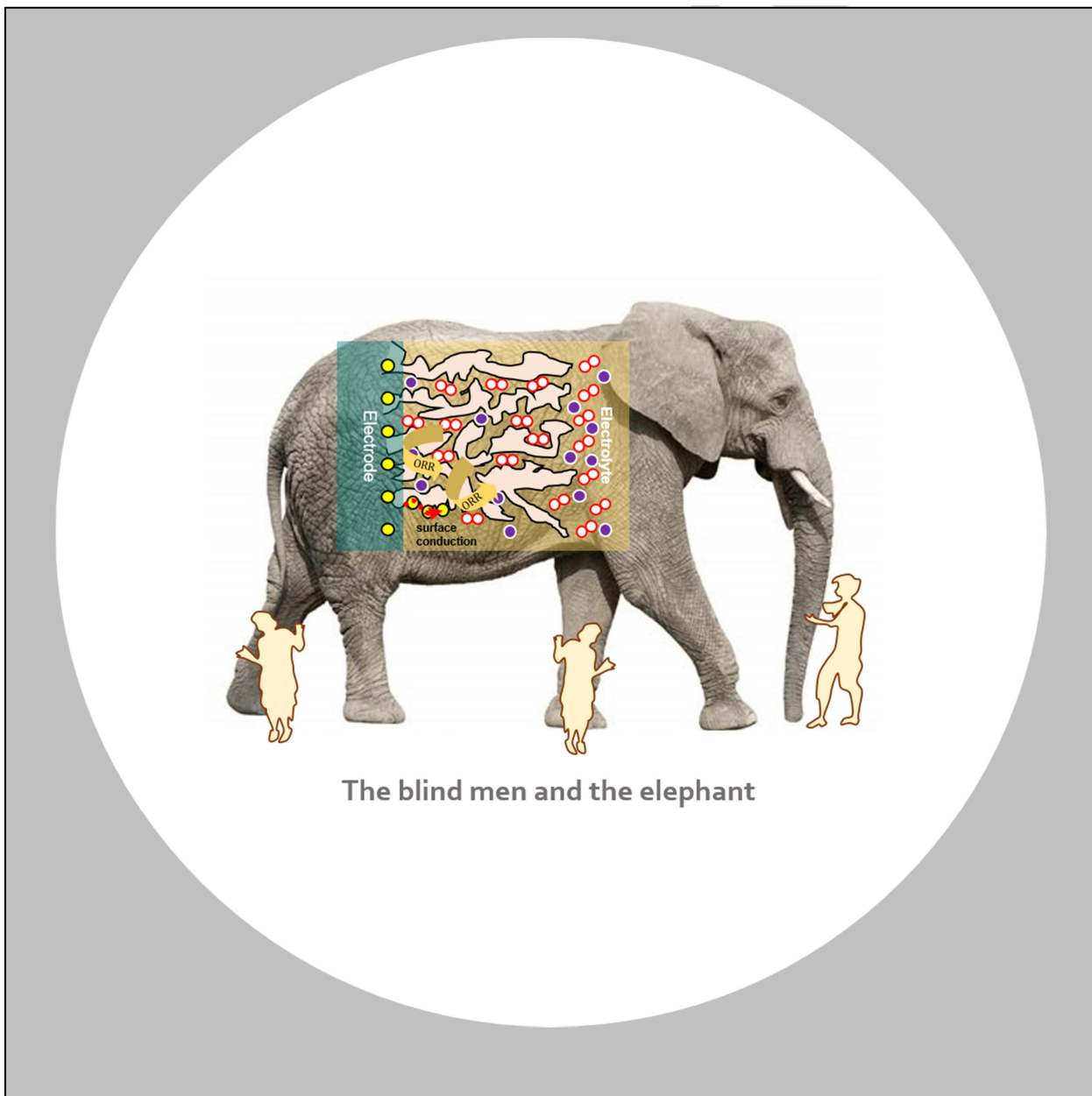


**VIP** Very Important Paper

# Understanding the Reaction Interface in Lithium-Oxygen Batteries

Jun Huang<sup>\*[a]</sup> and Zhangquan Peng<sup>\*[b]</sup>

The presented review article recapitulates the current state of the art in understanding three fundamental issues relevant to the reaction interface in lithium-oxygen batteries; i) charge transport across lithium peroxide, ii) morphological evolution and identification of reactive sites, and iii) mechanisms of the involved oxygen reactions. Except of the discharge reaction mechanism, there is still a lack of a complete mechanistic picture for these fundamental issues. However, we are standing at the brink of connecting the single dots to draw the overall

image. Neglect of double layer effects and nonlinearities has led us to stray from the path towards correct understanding of the charge transport. The current status of reaction sites reminds us of the parable of the blind and the elephant. Multiple *in-situ*, cross-validated methods and multiple working hypotheses are essential for a comprehensive understanding. More efforts, especially on identifying the reaction intermediates, are required to portray a unifying mechanistic scheme for the charge reaction mechanism.

## 1. Introduction

The electrode-electrolyte interface in batteries bring forth blessings and curses. The interface facilitates desirable reactions for generating/storing electricity, but at the same time, undesirable reactions occur, leading to degeneration of the functionality and even causing catastrophic outcomes in extreme cases. Decades of efforts in conceiving and designing better batteries strive to circumvent the following simple law: the interface that is more efficient in generating/storing electricity usually dies faster and is more dangerous in use.<sup>[1]</sup> As a consequence, it is not very bold to state that the battery science and technology is by and large an art of the interface.

In lithium-ion batteries, the most important interface is the solid-electrolyte interphase (SEI), formed mainly due to electrolyte decomposition on the electrode.<sup>[2]</sup> Usually, the SEI film has a bilayer structure consisting of an inner compact layer and an outer porous layer, as depicted in Figure 1.<sup>[2a]</sup> The porous layer, impregnated with electrolyte solution, allows electrolyte-phase transport of solvated Li<sup>+</sup> and anions. At the compact-porous interface, Li<sup>+</sup> ions undergo desolvation and proceed to transport in the compact layer. However, neither anions nor solvent molecules can penetrate through the compact layer.<sup>[3]</sup> Moreover, the compact layer is, in an ideal case, electrically insulative, thus preventing further decomposition of the electrolyte. At the interface between the electrode and the compact layer, Li<sup>+</sup> ions either deposit on the electrode surface or intercalate into the electrode material.

On the high end of the spectrum of energy density, lithium-oxygen batteries show a radically different type of interface, which is mainly composed of the discharge product Li<sub>2</sub>O<sub>2</sub> (Figure 1). Unlike the SEI in lithium-ion batteries with negligible inter-cycle structural variations, the Li<sub>2</sub>O<sub>2</sub> film in lithium-oxygen batteries forms and decomposes in every discharge-charge

cycle. In addition, being a wide-bandgap insulator, Li<sub>2</sub>O<sub>2</sub> imposes high barriers on charge transport.<sup>[4]</sup> As a result, charge transport across the Li<sub>2</sub>O<sub>2</sub> film is often regarded as the rate-determining step in lithium-oxygen batteries. In contrast, the rate-determining step in lithium-ion batteries is usually attributed to desolvation of Li<sup>+</sup> ions at the compact-porous interface.<sup>[5]</sup> A closer look at the interface in lithium-oxygen batteries immediately leads to the observation that the existence of the Li<sub>2</sub>O<sub>2</sub> film gives rise to three types of electrochemical interfaces in lithium-oxygen batteries; i) the electrode-electrolyte interface (at pristine state), ii) the Li<sub>2</sub>O<sub>2</sub>-electrolyte interface, and iii) the electrode-Li<sub>2</sub>O<sub>2</sub> interface. A natural question arises: which interface is involved in the oxygen reduction/evolution reaction (ORR/OER) upon discharge/charge, respectively.

The brief comparison presented above already touches on three key issues concerning the reaction interface in lithium-oxygen batteries; i) charge transport across the Li<sub>2</sub>O<sub>2</sub> film, ii) morphological evolution of the Li<sub>2</sub>O<sub>2</sub> film during discharge and charge, and iii) the ORR/OER mechanisms. These issues are discussed in this order in sections two to four. Section five summarizes the current understanding and discusses future challenges to address in order to lift some of the remaining secrets veiling the reaction interface in lithium-oxygen batteries.

## 2. Charge Transport

Interests in charge transport across the Li<sub>2</sub>O<sub>2</sub> film were instigated by the observation that at the end of discharge the cell voltage sharply drops off, which is often termed "sudden death" among researchers in this field. Hence, the discharge capacity delivered by porous carbon electrodes is far below the theoretical promise calculated using the electrode porosity.<sup>[4,6]</sup> The sudden death signifies mass transport limitations. Impeded oxygen transport caused by pore clogging is soon excluded as the major culprit as the same phenomenon is also observed on planar glass carbon electrodes in which case the oxygen transport limitation is greatly diminished.<sup>[6]</sup> Attention is therefore turned to the insulating Li<sub>2</sub>O<sub>2</sub> film, triggering an avalanche of both theoretical and experimental activities in this direction.<sup>[7]</sup>

There are broadly two schools on this topic. The electrochemical school led by Luntz advocates that the dominant charge transport mechanism is hole tunneling through the

[a] Prof. J. Huang  
Hunan Provincial Key Laboratory of Chemical Power Sources  
College of Chemistry and Chemical Engineering  
Central South University  
Changsha 410083, China  
E-mail: jhuangelectrochem@qq.com  
[b] Prof. Z. Peng  
State Key Laboratory of Electroanalytical Chemistry  
Changchun Institute of Applied Chemistry  
Chinese Academy of Science  
Changchun 130022, China  
E-mail: zqpeng@ciac.ac.cn

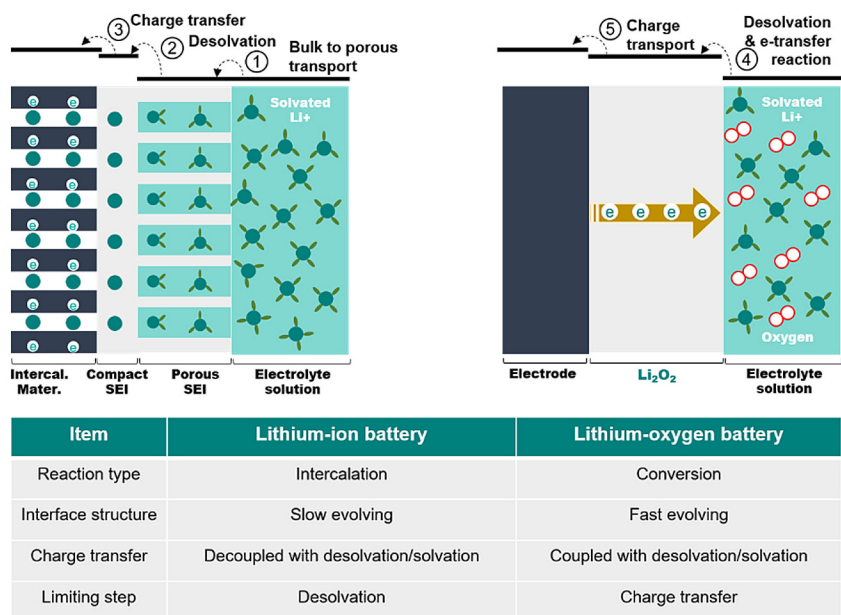


**Figure 1.** Comparison between the reaction interface in lithium-ion and lithium-oxygen batteries.

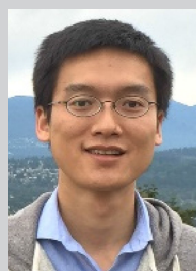
$\text{Li}_2\text{O}_2$  film.<sup>[4,7c,8]</sup> The most compelling evidence for this argument is that by introducing an outer-sphere redox shuttle, such as  $[\text{Fe}(\text{DMCp})_2]^{0/+}$ , into a discharged cell as an electrochemical probe of electron transfer across the  $\text{Li}_2\text{O}_2$  film, they observed that the charge transfer rate of the redox shuttle calculated using electrochemical impedance spectroscopy (EIS) attenuates exponentially with the discharge capacity (viz, the thickness of the  $\text{Li}_2\text{O}_2$  film).<sup>[4,9]</sup> The phenomenon observed can be well described by a classical theory, which gives out the following current-voltage relation [Eq. (1)] for electron tunneling effect across an insulating thin film,<sup>[10]</sup>

$$J_{\text{tun}} = j_0 \left( (E_t^0 + e\eta) e^{-A\sqrt{E_t^0 + e\eta}} - (E_t^0 + e\eta + e\Delta\phi) e^{-A\sqrt{E_t^0 + e\eta + e\Delta\phi}} \right) \quad (1)$$

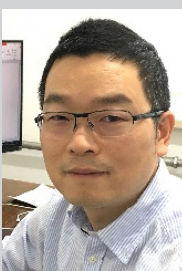
where  $j_0 = e/(2\pi h(\beta d)^2)$ ,  $A = (\sqrt{2m}4\pi\beta d)/h$ ,  $E_t^0$  the mean barrier height at equilibrium, a constant for a given material,  $\eta$

the overpotential (positive for discharge) associated with the  $\text{Li} - \text{O}_2$  redox,  $\Delta\phi$  the potential difference across the film,  $d$  the film thickness,  $\beta$  the correction factor,  $m$  the electron mass,  $e$  the electron charge,  $h$  the Planck's constant. Figure 2 (a) pictorially shows the band alignment in the  $\text{Li}_2\text{O}_2$  film and defines  $E_t^0$ ,  $\eta$  and  $\Delta\phi$ . The cell voltage during discharge is thus given by,  $U = E^{\text{eq}} - (\eta + \Delta\phi)$  with  $E^{\text{eq}}$  being the equilibrium potential.

It is readily seen from Eq.(1) that key factors determining  $J_{\text{tun}}$  include: (1)  $E_t^0$ , namely the gap between the valence band maximum (VBM) of  $\text{Li}_2\text{O}_2$  and the Fermi level  $\varepsilon_F$  of the  $\text{Li} - \text{O}_2$  redox.  $J_{\text{tun}}$  is greater at a lower  $E_t^0$ , which may explain why contaminants sometimes increase  $J_{\text{tun}}$ ,<sup>[11]</sup> (2) the cell voltage  $U$ , more specifically,  $\eta$  and  $\Delta\phi$ , according to  $U = E^{\text{eq}} - (\eta + \Delta\phi)$ .  $J_{\text{tun}}$  shall decrease at a lower  $U$  (namely, a higher discharge current density), explaining, in part, the premature sudden death observed during high-current-density discharge.<sup>[12]</sup> Moreover, hole tunneling shall be enhanced during charge ( $\eta < 0$ )



Huang Jun, obtained his Bachelor and PhD degrees in Tsinghua University in 2012 and 2017, respectively. During 2015–2016, he was a visiting PhD student in Michael Eikerling's research group at Simon Fraser University, working on the theory of Pt electrocatalysis. Since July 2017, he is associate professor at Central South University, and founds a research group focusing on the theory of electrocatalytic interfaces and reactions. He shows unabated interests in electrochemical impedance spectroscopy, especially in developing impedance models for data interpretation.



Peng Zhang-Quan, obtained his Bachelor degree in Wuhan University in 1997, and received his MSc and PhD degrees from Changchun Institute of Applied Chemistry (CIAC), Chinese Academy of Sciences (CAS) in 2000 and 2003, respectively. He continued by working as a postdoctoral researcher at University of Dusseldorf (Germany), University of Aarhus (Denmark) and University of St Andrews (United Kingdom) from 2004 to 2012. In 2012, he took a position as group leader of the Research Laboratory of Electrochemistry of Energy and Interface in CIAC. His current research interests are in-situ electrochemistry and computational electrochemistry focusing on Li-ion and  $\text{Li}_2\text{O}_2$  batteries.

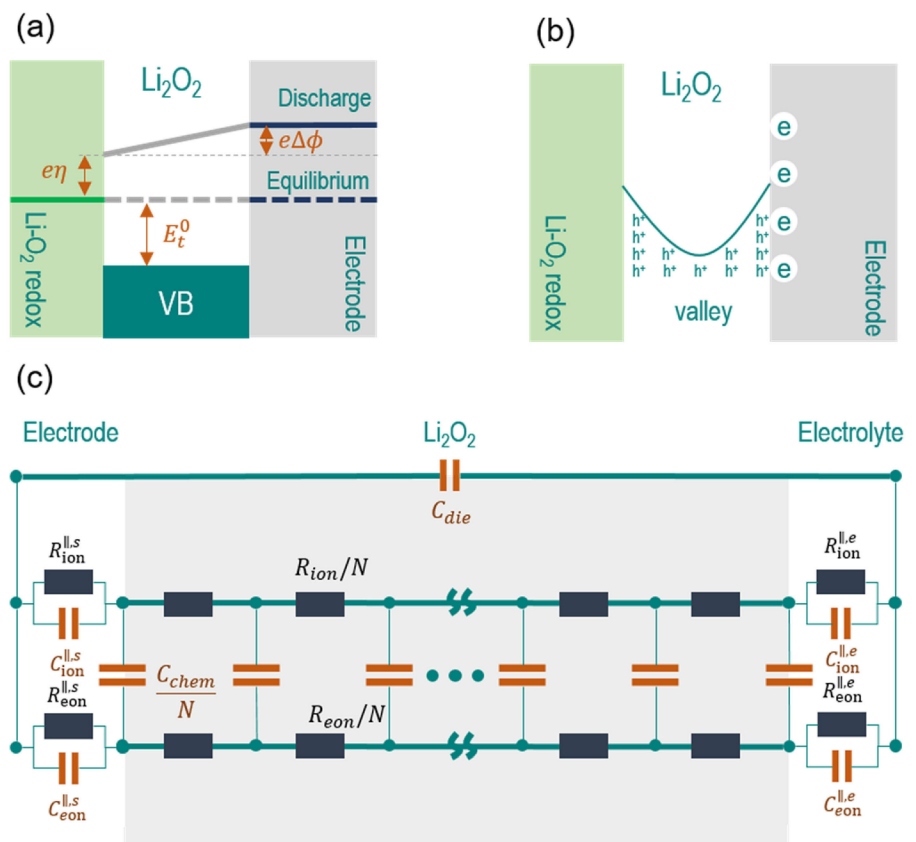


**Figure 2.** Charge transport across the  $\text{Li}_2\text{O}_2$  film. (a) Band alignment in the  $\text{Li}_2\text{O}_2$  film under equilibrium and discharge. (b) Double layer effects on the distribution of concentration of hole polarons. (c) Equivalent circuit mapping charge transport across the  $\text{Li}_2\text{O}_2$  film. The equivalent circuit has three rails corresponding to ion transport (denoted by the subscript 'ion', with  $R_{ion}$  being the ionic resistance), electron transport (denoted by the subscript 'eon', with  $R_{eon}$  being the electronic resistance), and electrical displacement (denoted by the subscript 'die', with  $C_{die}$  being the electrical capacitance of the film), respectively, along the transport coordinate.  $C_{chem}$  is the chemical capacitance, representing the ability to store chemical energy. The interfaces between the metal and  $\text{Li}_2\text{O}_2$  are represented by a parallel connection of interfacial resistances ( $R_{ion}^{||,s}$ ,  $R_{eon}^{||,s}$ ,  $R_{ion}^{||,e}$ ,  $R_{eon}^{||,e}$ , with the superscripts 's' and 'e' corresponding to the solid and electrolyte phase, respectively) and interfacial capacitances ( $C_{ion}^{||,s}$ ,  $C_{eon}^{||,s}$ ,  $C_{ion}^{||,e}$ ,  $C_{eon}^{||,e}$ ). The physical meanings of other symbols are explained in the main text.

according to our definition). Huang et al. is able to measure the resistance corresponding to charge transport across the  $\text{Li}_2\text{O}_2$  film at oxidative/reductive potentials using a dynamic electrochemical impedance spectroscopy (EIS) method,<sup>[13]</sup> and it is found that this charge transport resistance is lower at oxidative potentials than that at reductive potentials, which is consistent with the theoretical analysis; (3) the film thickness  $d$ .  $J_{tun}$  decreases exponentially (approximately as  $d$  also exists in the prefactor  $j_0$ ) with  $d$ . However,  $J_{tun}$  is independent on the temperature.<sup>[8]</sup>

The computational school represented by Siegel contends that the dominant mechanism is hopping of polarons and charged defects.<sup>[7a,b]</sup> In this view, the current density carried by hole-polarons is written as,

$$J_{hop} = eD_h \frac{\partial n_h(x)}{\partial x} + \frac{e^2 D_h n_h(x) \partial \phi(x)}{k_B T} \quad (2)$$

where  $D_h$  is the diffusion coefficient given by  $D_h = 2va^2 \exp(-E_{diff}/k_B T)$  with  $v$  being the hopping frequency,  $a$  the hopping distance,  $E_{diff}$  the diffusion barrier of hole polarons,  $n_h(x)$  the concentration of hole polarons,  $\phi(x)$  the

electrostatic potential. Under equilibrium,  $n_h(x)$  in bulk is given by,  $n_h^b = n_0 \exp(-E_t^0/k_B T)$  with  $n_0 \approx 3 \times 10^{22}$  site  $\text{cm}^{-3}$ .<sup>[8]</sup> Given that  $E_t^0 \approx 0.35$  eV, Luntz estimated that the Debye length  $\lambda_D \approx 85$  nm is larger than the thickness of the  $\text{Li}_2\text{O}_2$  film,<sup>[8]</sup> therefore,  $n_h(x)$  and  $\phi(x)$  are dictated by double layer effects, also termed space charge effects. Combining Eq.(2) with the Poisson equation,  $\varepsilon \nabla^2 \phi(x) = -\rho(x)$  with  $\rho(x)$  being the excess charge density, and assuming that hole-polarons are sole charge carriers, Radin et al. calculated  $n_h(x)$  in the  $\text{Li}_2\text{O}_2$  film, as schematically shown in Figure 2 (b).<sup>[7d]</sup> As  $n_h(x)$  significant varies across the  $\text{Li}_2\text{O}_2$  film, the ionic conductivity,  $\sigma_i(x) = z_i e^2 D_i n_i(x)/k_B T$  is also strongly spatially-dependent, and it is therefore insufficient to report a single-valued ionic conductivity for the  $\text{Li}_2\text{O}_2$  film.

Both mechanisms predict that charge transport is dependent, with the same trend but to different degree, on  $E_t^0$ :  $J_{tun} \sim E_t^0 \exp(-\sqrt{E_t^0})$  for the tunneling mechanism, while  $J_{hop} \sim \exp(-E_t^0)$  for the hopping mechanism. As a result, bringing the Fermi level  $\varepsilon_F$  of the  $\text{Li}-\text{O}_2$  redox closer to the VBM of  $\text{Li}_2\text{O}_2$ , that is, decreasing  $E_t^0$ , will promote the hopping mechanism, compared with the tunneling mechanism, to a greater extent. Luntz et al. argued that  $J_{tun} \sim \exp(-d)$  while

$J_{hop} \sim d^{-1}$  and we can make use of this difference to tell apart these two mechanisms.<sup>[8,11]</sup> However, these two relations, especially the latter, are questionable, because  $d$  also changes the prefactor  $j_o$  in  $J_{tun}$  and the assumption for the latter relation that  $n_h(x)$  and  $\phi(x)$  are linear distributions in the  $\text{Li}_2\text{O}_2$  film is in no way accurate. By considering double layer effects, Radin et al. reveals that  $J_{hop}$  decreases with  $d$  more significantly than the  $J_{hop} \sim d^{-1}$  relation.<sup>[7d]</sup> Luntz et al. further pointed out that the contrast that  $J_{hop}$  is temperature-independent while  $J_{hop}$  increases at higher temperatures can be harnessed to distinguish these two contributions.<sup>[8,11]</sup>

Luntz et al. challenged that the hopping mechanism cannot be the dominant mechanism under normal conditions because the relation  $J_{hop} \sim d^{-1}$  cannot explain the sudden death.<sup>[11]</sup> As a response, Siegel et al. argued that by taking into account double layer effects the sudden death is explicable in the spirit of the hopping mechanism: the concentration of charge carriers in the middle plane of the  $\text{Li}_2\text{O}_2$  film is too low to carry the required current density when the  $\text{Li}_2\text{O}_2$  film is very thick, as schematically shown in Figure 2 (b).<sup>[7d]</sup> Siegel et al.<sup>[7d]</sup> and Monroe et al.<sup>[14]</sup> pointed out that the tunneling mechanism which predicts an approximately exponential dependence of charge transport resistance on  $d$  is at odds with the observation that the cell voltage linearly declines during discharge before the sudden death. Luntz et al. corresponded with the speculation that scattering of tunneling holes caused by charged vacancies is responsible for this linear decrease.<sup>[7c]</sup> Writing in a recent review paper, Siegel et al. quotes the viewpoint of Luntz et al., namely the hole-tunneling mechanism, as the dominant charge transport mechanism.<sup>[15]</sup> Nevertheless, they concluded that neither mechanism appears to be capable of providing the current density observed in experiments.<sup>[15]</sup>

Experimental measurement of charge transport across the  $\text{Li}_2\text{O}_2$  film is rare and usually employs the EIS method. Gerbig et al. employed a cell configuration of metal| $\text{Li}_2\text{O}_2$ |metal to study the electronic and ionic conductivity of  $\text{Li}_2\text{O}_2$ .<sup>[16]</sup> In this cell configuration, the charge transport through  $\text{Li}_2\text{O}_2$  can be well represented by an equivalent circuit shown in Figure 2 (c), which is a direct map of the physics underpinning the charge transport process.<sup>[17]</sup> Lai and Haile gave a lucid exposition on this mapping process.<sup>[18]</sup> The equivalent circuit has three rails corresponding to ion transport (mapped from Nernst-Planck equation for ions), electron transport (mapped from Nernst-Planck equation for electrons), and electrical displacement (mapped from Poisson equation), respectively, along the transport coordinate. The differential resistance along the ionic and electronic rail,  $R_{ion}/N$  and  $R_{eon}/N$  with  $N$  being the number of differential units, should be spatially-dependent with reasons explained before. There are two capacitances, an electrical one  $C_{die} = \epsilon/d$  corresponding to the ability to store electrical energy, and a chemical one  $C_{chem} = \frac{\epsilon^2}{k_B T} \left( \frac{1}{C_{ion}} + \frac{1}{C_{eon}} \right)^{-1} d$  corresponding to the ability to store chemical energy.<sup>[17c]</sup>  $C_{chem}$  dominates over  $C_{die}$  for thick films. Each interface between the metal and  $\text{Li}_2\text{O}_2$  is represented by a parallel connection of an interfacial resistance and an interfacial capacitance. The value of the interfacial resistance reflects the reactivity of the interface,

e.g., an infinite interface resistance corresponds to a blocking electrode.

When we neglect double layer effects and assume that circuit elements  $R_{eon}$ ,  $R_{ion}$  and  $C_{chem}$  are uniform across the  $\text{Li}_2\text{O}_2$  film, the equivalent circuit in Figure 2 (c) is amenable to analytical solutions, which are then employed to fit the EIS data.<sup>[17c,18]</sup> Ionic and electronic conductivity are purportedly separated, and it is found in several studies that the electronic conductivity is several orders lower than the ionic conductivity, and both depend on the crystallinity of  $\text{Li}_2\text{O}_2$ .<sup>[16]</sup> As aforementioned, transport through the  $\text{Li}_2\text{O}_2$  film is governed by double layer effects, leading to significant distributions of  $n_h(x)$  and  $\phi(x)$ , thus, defying the assumption that  $R_{eon}$ ,  $R_{ion}$  and  $C_{chem}$  are uniform. Keeping this in mind, one should caution the reliability of charge transport properties extracted from EIS data under the assumption of uniform  $R_{eon}$ ,  $R_{ion}$  and  $C_{chem}$ . Let's put in another way, conductivity, being spatially-dependent, is not the desirable descriptor for charge transport in mixed conducting thin films that are governed by double layer effects.

Only until recent has nonlinearity been considered in understanding charge transport across the  $\text{Li}_2\text{O}_2$  film.<sup>[19]</sup> Analysis based on Eq. (2) is valid within the linear (near-equilibrium) regime. As the  $\text{Li}_2\text{O}_2$  film is thinner or comparable to the Debye length, there will be, however, strong electric field in the  $\text{Li}_2\text{O}_2$  film, in which case nonlinearities shall play an important role. A simple analysis carried by Kaiser et al. demonstrated the importance of nonlinearities, being that the exponential increase of the charge transport resistance can be rationalized by nonlinear hopping.<sup>[19]</sup> However, this analysis is far from being self-consistent in that the nonlinear ion transport law is fed with a linear potential distribution for the sake of analytical solutions.

In summary, concerted efforts from both experimental and theoretical sides have generated considerable understanding towards charge transport in the  $\text{Li}_2\text{O}_2$  film, while this endeavor is, though, far from being complete. A mechanism that is able to explain both the linear and the sudden-death regimes during discharge is yet to come. The ultra-thin nature of  $\text{Li}_2\text{O}_2$  brings forth strong fields, rendering that nonlinearities and double layer effects cannot be neglected. Moreover, as the conductivity is spatially dependent, reporting a single-valued conductivity is of limited information or even misleading for the  $\text{Li}_2\text{O}_2$  film.

### 3. Reaction Sites

Identifying the reaction site lays the basis for understanding the reaction mechanism and improving the cell performance. There are multiple plausible types of reaction sites: the interface between the  $\text{Li}_2\text{O}_2$  film and the electrolyte, the interface between the electrode surface and the  $\text{Li}_2\text{O}_2$  film, and the interface between the electrode surface and the electrolyte (when the electrode surface is not fully covered by  $\text{Li}_2\text{O}_2$ ). Each kind of reaction site involves a distinct reaction route. For example, transport of  $\text{Li}^+$  and oxygen across the  $\text{Li}_2\text{O}_2$  film are involved if ORR occurs at the electrode- $\text{Li}_2\text{O}_2$  interface, while electrons need to transport across the  $\text{Li}_2\text{O}_2$  film if ORR occurs

at the  $\text{Li}_2\text{O}_2$ -electrolyte interface. There are heated controversies over this fundamental question. In next paragraphs, we will recapitulate findings obtained first from in-situ morphology techniques and then from electrochemical techniques.

In-situ morphology techniques can provide visualized information of the reaction site; however, sharply different views prevail in the literature. Figure 3 summarizes representative studies in this direction. In 2013, Zhong et al. employed in-situ transmission electron microscopy (TEM) to investigate the oxidation of a  $\text{Li}_2\text{O}_2$  particle supported on a multi-walled carbon nanotube (MWCNT) in a solid state  $\text{Li}-\text{O}_2$  battery.<sup>[20]</sup> A delithiated Si nanowire coated with  $\text{LiAlSiO}_x$  (solid electrolyte) was used as the negative electrode. Note that the MWCNT-coated  $\text{Li}_2\text{O}_2$  particle was electrochemically formed in a previous discharge experiment and then transferred to the TEM microbattery. It is revealed that  $\text{Li}_2\text{O}_2$  decomposition begins at the CNT- $\text{Li}_2\text{O}_2$  interface, indicating that  $\text{Li}_2\text{O}_2$  oxidation is limited by electron transport. This conclusion is further corroborated by the observation that the part of a  $\text{Li}_2\text{O}_2$  particle having more facile access to electron transport is decomposed earlier and faster.

Zheng et al.,<sup>[21]</sup> observing different phenomena as to be discussed below, hypothesized that there is possible contamination during microbattery construction and transfer in the work of Zhong et al. Another noteworthy factor is that a very high voltage of 10 V was applied between the MWCNT-coated  $\text{Li}_2\text{O}_2$  and the negative electrode. Recalling charge transport mechanisms discussed in the preceding section, one must caution that such high voltage will dramatically change the charge transport properties, as a consequence, the phenomena observed may be very different from what happens in a real lithium-oxygen battery, and the knowledge obtained cannot be directly transferred to realistic cases. This is unfortunately the common deficiency of most in-situ morphological studies.

Later on, armed with environmental scanning electron microscope (ESEM), Zheng et al. was able to probe both discharge and charge process of a solid-state lithium-oxygen battery.<sup>[21]</sup> During discharge, formation of hollow spheres is initiated at the CNT-solid electrolyte ( $\text{Li}_2\text{O}$ )-oxygen triple phase interface (TPI). In the later stage of discharge, new  $\text{Li}_2\text{O}_2$  particles, remote from the electrode surface, are formed on

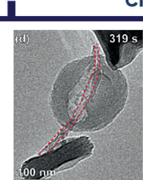
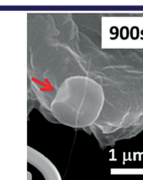
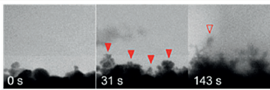
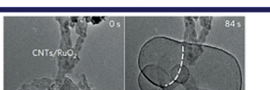
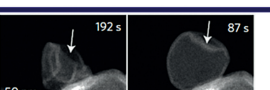
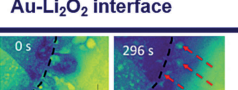
Source	Method	Discharge	Charge	Comment
2013 Zhong et al.	MWCNT/ $\text{Li}_2\text{O}_2$ - $\text{LiAlSiO}_x$ -Si NW all solid state cell  In-situ TEM	Discharged in an electrochemical cell; $\text{Li}_2\text{O}_2$ is then transferred to the TEM cell	(d)  319 s 100 nm	Electron- transport- limited  Possible contamination during microbattery construction and transfer  Decomposition begins at the center of the $\text{Li}_2\text{O}_2$ particle
2014 Zheng et al.	SACNT- $\text{Li}_2\text{O}_2$ - Li all solid state cell  Environmental SEM	(d)  500 nm	Li $_2\text{O}_2$ formation prefers at the triple phase interface  900 s 1 μm	Occurs on the large bare surface area where it is favorable for the oxygen release  Very large overpotential during discharge/charge (exceeding 5 V) greatly changes the charge transport properties  Unexpected toroid shape
2015 Kushima et al.	Au-DMSO liquid cell  In-situ TEM	 Porous layer formed on $\text{Li}_2\text{O}_2$ -electrolyte interface	 Decomposition occurs on Au- $\text{Li}_2\text{O}_2$ interface	Lacking of compositional identification  Baffling porous structure formation under high overpotential discharge
2017 Luo et al.	CNT- $\text{Li}_2\text{O}_2$ -Li solid state cell  Environmental TEM	 Hollow sphere $\text{Li}_2\text{O}_2$ formed at the triple phase interface	 Collapse begins at sites far from the electrode surface	$\text{Li}_2\text{O}_2$ formation away from the triple phase interface is observed  Disproportionation of $\text{LiO}_2$ releases $\text{O}_2$ , causing hollow sphere structure
2018 Liu et al.	Au-DMSO liquid cell  HAADF-STEM	a  h 	i  j 	Constant current density ( $1.3 \mu\text{A cm}^{-2}$ ) discharging/charging  Current density dependence is not studied
2018 He et al.	GC-TEGDME liquid cell  STEM	0 s  34 s 	0 s  296 s 	Constant potential discharging(-2.5 V) charging (2.5 V)  $\text{Li}_2\text{O}_2$ particles in electrolyte are oxidized

Figure 3. Application of in-situ morphology techniques to visualize the reaction interface in lithium-oxygen batteries.

previous  $\text{Li}_2\text{O}_2$  particles. Upon recharge, collapse of spherical  $\text{Li}_2\text{O}_2$  particles occurs on the bare surface that is not in contact with the CNT. Those observations point to the conclusion that the electron and ion transport capability of  $\text{Li}_2\text{O}_2$  is sufficient to form and decompose  $\text{Li}_2\text{O}_2$  at sites remote from the electrode surface. Note again that a voltage of  $-3\text{ V}$  was applied on the CNT vs a Li metal anode during discharge, and a voltage of  $8\text{ V}$  during recharge. In 2017, Luo et al. arrived at similar conclusions for a solid-state lithium-oxygen battery by employing in-situ TEM.<sup>[22]</sup>

The first in-situ visualization of the discharge/charge process of a liquid lithium-oxygen cell, which better emulates lithium-oxygen batteries, was accomplished by Kushima et al. in 2016.<sup>[23]</sup> The working electrode is Au and the electrolyte is  $1.0\text{ M}$  (trifluoromethane)sulfonimide salt ( $\text{LiTFSI}$ ) dissolved in dimethyl sulfoxide (DMSO). Upon discharge at  $-3.5\text{ V}$  vs the anode, nanoscale particles are formed on the Au electrode. As the discharge reaction proceeds, new particles are formed on the top of previous particles, indicating that the ORR occurs on the  $\text{Li}_2\text{O}_2$ -electrolyte interface, rather than the electrode- $\text{Li}_2\text{O}_2$  or electrode- electrolyte interface. These particles accumulate, leading to the growth of a porous film, which is, intriguingly, self-limiting in that its thickness ceases to grow beyond  $100\text{ nm}$  and further discharge results in filling of the pores with newly formed particles. The film thickness exceeds the limiting thickness predicted by the hole tunneling mechanism ( $5\text{--}10\text{ nm}$ ), and surface conduction is invoked to explain  $\text{Li}_2\text{O}_2$  formation remote from the electrode. It is difficult, however, to identify the exact composition of the particles formed during discharge. Upon recharge at  $1.5\text{ V}$  vs the anode, it is observed that voids are formed in the discharge product film near the Au electrode, indicating that the recharge reactions occur at the electrode- $\text{Li}_2\text{O}_2$  interface. Combined, Kushima et al. reported that the  $\text{Li}_2\text{O}_2$  layer is porous, and the reaction site is asymmetrical during discharge and charge, which is believed to be the underlying causes of the baffling asymmetry in the cell overpotentials during discharge and charge.

Two subsequent studies in 2018 in the liquid cell configuration observed similar phenomena. Employing scanning transmission electron microscopy with enhanced contrast by a high angle annular dark field (HAADF-STEM), Liu et al. observed that a porous  $\text{Li}_2\text{O}_2$  film up to  $160\text{ nm}$  is formed on the Au electrode immersed in  $1.0\text{ M}$   $\text{LiClO}_4$  in dimethylsulfoxide (DMSO).<sup>[24]</sup> This study represents the first in-situ visualization of the cell under a constant current density ( $1.3\text{ }\mu\text{A cm}^{-2}$ ). However, the experiments were conducted with only one current density, and the informative current dependency of the interfacial morphology is not examined yet. In addition, the discharge curve does not, though, show sudden death. Upon recharge, it is also found that decomposition of  $\text{Li}_2\text{O}_2$  begins at the Au- $\text{Li}_2\text{O}_2$  interface. In the late stage of charge,  $\text{Li}_2\text{O}_2$  particles that are up to  $160\text{ nm}$  away from the Au electrode are decomposed. He et al. applied in-situ liquid TEM to observe the discharge/charge of a glass carbon (GC) electrode in  $1\text{ M}$   $\text{LiCF}_3\text{SO}_2$  in TEGDME.<sup>[25]</sup> The same phenomena that a porous  $\text{Li}_2\text{O}_2$  film is formed during discharge and decomposition of  $\text{Li}_2\text{O}_2$  occurs at the GC-  $\text{Li}_2\text{O}_2$  interface are observed.

Albeit providing visualized information, in-situ advanced morphology techniques are conducted on modified systems that are substantially different from the realistic lithium-oxygen batteries. On the contrary, in-situ, non-invasive electrochemical methods can be applied to systems more alike the realistic lithium-oxygen batteries.

In 2012, McCloskey et al. employed isotope-labeled differential electrochemical mass spectrometry (DEMS) to study the reaction interface in lithium-oxygen batteries.<sup>[26]</sup> A lithium-oxygen cell with  $1\text{ M}$   $\text{LiBF}_4$ /DME as the electrolyte was discharged under  $^{18}\text{O}_2$  and then  $^{16}\text{O}_2$  atmosphere. Upon recharge,  $^{16}\text{O}_2$  generated from  $\text{Li}_2\text{O}_2$  that was formed in the latter stage of discharge dominates in the low overpotential stage, while  $^{18}\text{O}_2$  generated from  $\text{Li}_2\text{O}_2$  that was formed in the earlier stage of discharge dominates in the high overpotential stage. In 2016, Wang et al. applied in-situ surface-enhanced Raman spectroscopy (SERS) to tract the compositional evolution of the reaction interface.<sup>[27]</sup> An Au electrode in  $0.1\text{ M}$   $\text{LiClO}_4$ /DMSO was passivated using  $^{18}\text{O}_2$  and then subjected to discharge under  $^{16}\text{O}_2$ . In SERS the signal of  $\text{Li}_2^{18}\text{O}_2$  is gradually replaced with that of  $\text{Li}_2^{16}\text{O}_2$ . Upon recharge,  $\text{Li}_2^{16}\text{O}_2$  formed in the latter stage is earlier to decompose. This observation is fully consistent with that from McCloskey et al. It is speculated that both ORR and OER occur on the electrode- $\text{Li}_2\text{O}_2$  interface. This conclusion is based on a tacit assumption that the  $\text{Li}_2\text{O}_2$  film uniformly covers the electrode surface, which is not necessarily the case as known from above in-situ morphology studies. If the  $\text{Li}_2\text{O}_2$  film is porous and non-uniform and has a thickness up to  $100\text{ nm}$ , other schemes could also explain the DEMS and SERS results. For example, the previously formed  $\text{Li}_2^{18}\text{O}_2$  is gradually covered (rather than displaced) by the newly formed  $\text{Li}_2^{16}\text{O}_2$ , which can certainly be formed at the  $\text{Li}_2\text{O}_2$ -electrolyte interface, resulting in the declining  $\text{Li}_2^{18}\text{O}_2$  signal in SERS. In addition, it is important to note that  $^{18}\text{O}_2$  is also generated immediately upon recharge in the work of McCloskey et al., though its rate is slower than  $^{16}\text{O}_2$ , implying that the  $\text{Li}_2\text{O}_2$  film interfacing the electrode is non-uniform but composed of both  $\text{Li}_2^{18}\text{O}_2$  and  $\text{Li}_2^{16}\text{O}_2$ .

EIS was employed by Huang et al. to interrogate the reaction interface.<sup>[13,28]</sup> In an earlier study, EIS at a pristine electrode and that on a fully discharged electrode were compared.<sup>[28]</sup> It is found that only one semicircle corresponding to oxygen reaction is observed in the EIS at a pristine electrode, while two semicircles are observed in the EIS at a discharged electrode. The same phenomenon was confirmed in a separate study by Kaiser et al.<sup>[19]</sup> The new semicircle in the high-frequency range is assigned to charge transport, mainly electron transport, across the  $\text{Li}_2\text{O}_2$  film formed during discharge. This structural transformation, implying that electrons need to transport across the  $\text{Li}_2\text{O}_2$  film to participate in the ORR, leads Huang et al. to conclude that the ORR occurs on the  $\text{Li}_2\text{O}_2$ -electrolyte interface, which is corroborated with physics-based EIS modeling. In a latter study, Huang et al. applied dynamic EIS that is measured during potentiostatic/galvanostatic discharge/charge to probe the dynamics of the reaction interface in lithium-oxygen batteries.<sup>[13]</sup> During discharge, EIS again transforms from single-semicircle structure at pristine state to two-semicircle structure after discharge, with

the high-frequency semicircle growing in an exponential manner, namely the charge transport resistance grows exponentially as a function of the discharged capacity. Intriguing, the high-frequency semicircle disappears upon recharge, which is taken as the signal of the transformation of the reaction interface from the  $\text{Li}_2\text{O}_2$ -electrolyte interface to the electrode- $\text{Li}_2\text{O}_2$  interface. Note again that the conclusions made by Huang et al. also bear the assumption that the  $\text{Li}_2\text{O}_2$  film is compact and uniform. Although care was taken to fulfill this assumption by using a very high discharge current density, the morphology of the  $\text{Li}_2\text{O}_2$  film was never visualized anyhow.

Figure 4 recapitulates current understandings toward the reaction site in lithium-oxygen batteries. There are broadly three cases: OER/ORR occurs at the  $\text{Li}_2\text{O}_2$ -electrolyte interface in (a) and (d), OER/ORR occurs at the electrode- $\text{Li}_2\text{O}_2$  interface in (b) and (e), as well as the  $\text{Li}_2\text{O}_2$  layer is porous and OER/ORR occurs at both the electrode- $\text{Li}_2\text{O}_2$  interface and the electrode- $\text{Li}_2\text{O}_2$  interface assisted by surface conduction in (c) and (f). Moreover, for the case of a porous  $\text{Li}_2\text{O}_2$  film, intermediates formed from reactions occurring at the electrode- $\text{Li}_2\text{O}_2$  interface can dissolve into the electrolyte and transport to reaction sites far away ( $\sim 100$  nm) from the electrode surface. We will return back to this point in the next section on reaction mechanisms.

There is growing consensus on asymmetrical reaction sites during discharge and charge. Specifically, ORR occurs on the  $\text{Li}_2\text{O}_2$ -electrolyte interface during discharge, while OER occurs on the electrode- $\text{Li}_2\text{O}_2$  interface during recharge. The plausible argument that ORR occurs on the electrode- $\text{Li}_2\text{O}_2$  interface may be encountered with difficulties in ensuring consistency with the observation that the reaction pathway of ORR is heavily dependent on the solution properties, as to be discussed in detail in the next section. According to the discussion on charge transport in the preceding section, we know that charge

transport capability of  $\text{Li}_2\text{O}_2$  shall be improved during charge compared to discharge. One may then wonder why the charge overpotential is much higher than discharge overpotential and why the reaction site needs to transform to the electrode- $\text{Li}_2\text{O}_2$  interface if the charge transport limitation is less significant for recharge. Luntz et al. found that the intrinsic kinetics of  $\text{Li}_2\text{O}_2$  oxidation is not as sluggish as most believe, and the high overpotential seen in the latter stage of charge is attributed to electrolyte decomposition.<sup>[29]</sup> Regarding the latter doubt, although charge transport across  $\text{Li}_2\text{O}_2$  is improved during recharge, OER prefers the electrode- $\text{Li}_2\text{O}_2$  interface, in which case electron transport cross  $\text{Li}_2\text{O}_2$  is no longer involved at all.

Although substantial understandings have been achieved, the reaction sites in lithium-oxygen batteries are still controversial. A conclusive picture is yet to come. Only by combining multiple complementary techniques (in-situ morphology techniques and electrochemical spectroscopic methods) can we get closer to the truth. Moreover, intricacies on how the electrode materials, the electrolyte recipe and operating conditions (e.g., the current density) impact the reaction site remain largely unknown.

#### 4. Reaction Mechanism

Fundamental research in the past decade has generated considerable understanding of ORR mechanisms during discharge, which is further transformed to practical approaches to boost the discharge capacity. On the contrary, reaction mechanism during recharge remains elusive and controversial, which is, in part, responsible for the fact that lithium-oxygen batteries are limited by the capability of recharge.

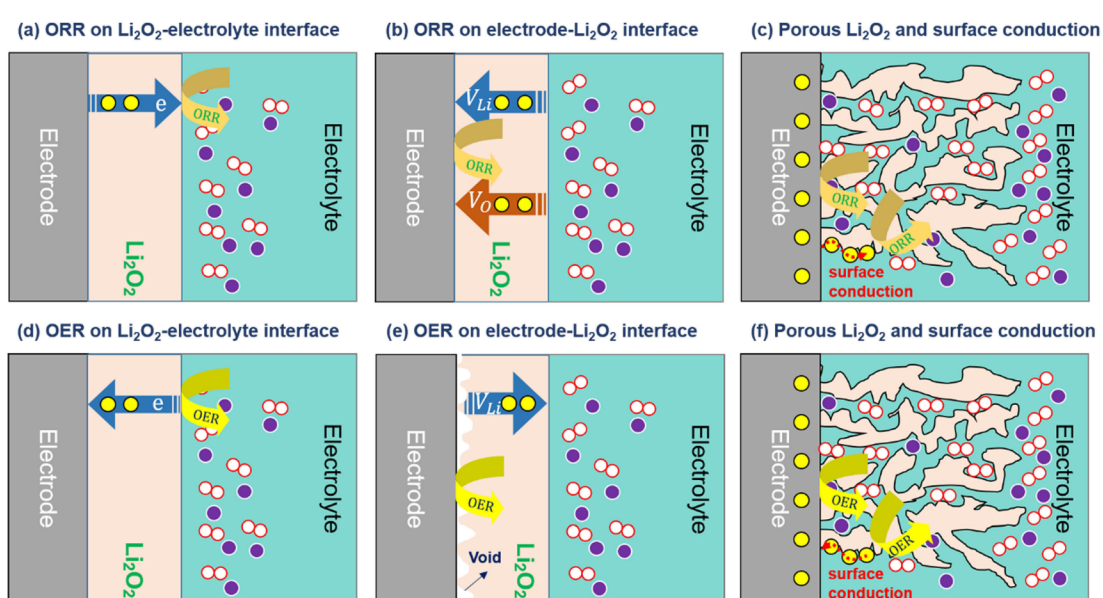


**Figure 4.** OER/ORR occurs at the  $\text{Li}_2\text{O}_2$ -electrolyte interface in (a) and (d), OER/ORR occurs at the electrode- $\text{Li}_2\text{O}_2$  interface in (b) and (e), as well as the reaction interface is porous and OER/ORR occurs at multiple sites, namely the electrode- $\text{Li}_2\text{O}_2$  interface and the electrode- $\text{Li}_2\text{O}_2$  interface assisted by surface conduction in (c) and (f).

Figure 5 shows pictorially the widely-accepted mechanism of discharge reactions.<sup>[30]</sup> The first step is adsorption of O<sub>2</sub> on the electrode surface, O<sub>2</sub> + \* → O<sub>2</sub><sup>\*</sup> (\* represents an active site), followed by an electron transfer step, O<sub>2</sub><sup>\*</sup> + e → O<sub>2</sub><sup>−</sup>. Afterwards, the superoxide anion (O<sub>2</sub><sup>−</sup>) either combines with a Li<sup>+</sup> forming LiO<sub>2</sub><sup>\*</sup> (adsorbed lithium superoxide), O<sub>2</sub><sup>−</sup> + Li<sup>+</sup>(sol)<sub>n</sub> → LiO<sub>2</sub><sup>\*</sup> + n · sol, or dissolves into the electrolyte solution forming O<sub>2</sub><sup>−</sup>(sol)<sub>m</sub> and releasing an active site, O<sub>2</sub><sup>−</sup> + m · sol → O<sub>2</sub><sup>−</sup>(sol)<sub>m</sub> + \*. Solvent molecules play a role in above two steps. Formation of LiO<sub>2</sub><sup>\*</sup> takes off the solvation shell of Li<sup>+</sup>(sol)<sub>n</sub>, while dissolution of O<sub>2</sub><sup>−</sup> takes along several solvent molecules. LiO<sub>2</sub><sup>\*</sup> is then transformed, through a Li<sup>+</sup>-coupled electron transfer step, to lithium peroxide residing on the electrode surface, LiO<sub>2</sub><sup>\*</sup> + Li<sup>+</sup>(sol)<sub>n</sub> + e → Li<sub>2</sub>O<sub>2</sub> + \* + n · sol. An active site may be released in the above step, as oxygen is assumed to be able to adsorb onto the Li<sub>2</sub>O<sub>2</sub> surface when the Li<sub>2</sub>O<sub>2</sub>–electrolyte interface is viewed as the reaction interface. As long as O<sub>2</sub><sup>−</sup>(sol)<sub>m</sub> is considered, it combines with an Li<sup>+</sup>(sol)<sub>n</sub> forming LiO<sub>2</sub>, O<sub>2</sub><sup>−</sup>(sol)<sub>m</sub> + Li<sup>+</sup>(sol)<sub>n</sub> → LiO<sub>2</sub> + (m + n) · sol, and then LiO<sub>2</sub> disproportionates forming Li<sub>2</sub>O<sub>2</sub>, LiO<sub>2</sub> + LiO<sub>2</sub> → Li<sub>2</sub>O<sub>2</sub> + O<sub>2</sub>. Recently, singlet oxygen ('O<sub>2</sub>) generated from the oxygen disproportionation of LiO<sub>2</sub> is identified as the major culprit for performance degradation in lithium-oxygen batteries.<sup>[35]</sup> Note that LiO<sub>2</sub> may also carry a solvation shell, on which we have little if any knowledge currently.

It is readily seen that the electrolyte solvent (solvation and desolvation), the electrode potential (electron transfer) and the electrode surface properties (surface adsorption) are key factors dictating the discharge reaction. A simple thermodynamic analysis given below, in which the formation free energy of O<sub>2</sub><sup>−</sup>, LiO<sub>2</sub><sup>\*</sup> and O<sub>2</sub><sup>−</sup>(sol)<sub>m</sub> are key descriptors, will give us a grip on understanding the trends.

Taking gaseous oxygen as the energy reference, the formation free energy of O<sub>2</sub><sup>−</sup> is actually free energy of the reaction, O<sub>2</sub> + \* + e → O<sub>2</sub><sup>−</sup>, which is given by,

$$\Delta G_{O_2^{\cdot-}} = \Delta G_{O_2^{\cdot-}}^0 + RT \cdot \ln \left( \frac{\theta_{O_2^{\cdot-}} p_{O_2}^{\text{ref}}}{(1 - \theta_{O_2^{\cdot-}} - \theta_{LiO_2^{\cdot}}) p_{O_2}} \right) + F(\phi^M - \phi^S) \quad (3)$$

where  $\Delta G_{O_2^{\cdot-}}^0 = G_{O_2^{\cdot-}}^0 - G_{O_2}^0 - G_{\cdot}^0 - G_e^0$ , with

$G_X^0$  ( $X = O_2^{\cdot-}, O_2, \cdot, e$ ) being the electrochemical energy of  $X$  under the standard state, is the standard adsorption energy of O<sub>2</sub><sup>−</sup>, a quantity depending on the electrode surface properties,  $\theta_X$  ( $X = O_2^{\cdot-}, LiO_2^{\cdot}$ ) is the coverage of surface adsorbates,  $p_{O_2}$  is the oxygen pressure,  $p_{O_2}^{\text{ref}}$  is the reference oxygen pressure,  $\phi^M$  is the electrode potential,  $\phi^S$  is the solution phase potential at the adsorbate plane. Other variables have their usual meanings. More negative  $\Delta G_{O_2^{\cdot-}}$ , such as by lowering  $\phi^M$ , means that formation of O<sub>2</sub><sup>−</sup> is preferable.

In the similar manner, the formation free energy of LiO<sub>2</sub> and O<sub>2</sub><sup>−</sup>(sol)<sub>m</sub> are actually free energy of the reactions, O<sub>2</sub> + e + m · sol → O<sub>2</sub><sup>−</sup>(sol)<sub>m</sub> and O<sub>2</sub> + e + Li<sup>+</sup>(sol)<sub>n</sub> + \* → LiO<sub>2</sub><sup>\*</sup> + n · sol, respectively, which are written as,

$$\Delta G_{O_2^{\cdot-}(\text{sol})_m} = \Delta G_{O_2^{\cdot-}}^0 + \Delta G_{O_2^{\cdot-}}^0 + RT \cdot \ln \left( \frac{p_{O_2}^{\text{ref}}}{p_{O_2}} \right) + F(\phi^M - \phi^S) \quad (4)$$

$$\Delta G_{LiO_2^{\cdot}} = -\Delta G_{Li^+}^{\text{sol}} + D_{LiO_2^{\cdot}} + \Delta G_{O_2^{\cdot-}}^0 + RT \cdot \ln \left( \frac{\theta_{LiO_2^{\cdot}} p_{O_2}^{\text{ref}} c_{Li^+}^{\text{ref}}}{(1 - \theta_{O_2^{\cdot-}} - \theta_{LiO_2^{\cdot}}) p_{O_2} c_{Li^+}} \right) + F(\phi^M - \phi^S) \quad (5)$$

where  $\Delta G_{O_2^{\cdot-}}^{\text{sol}} = G_{O_2^{\cdot-}(\text{sol})_m}^0 + G_{\cdot}^0 - G_{O_2^{\cdot-}}^0 - mG_{\text{sol}}$  is the solvation energy of O<sub>2</sub><sup>−</sup>, which is more negative for a stronger solvation of O<sub>2</sub><sup>−</sup>,  $\Delta G_{Li^+}^{\text{sol}} = G_{Li^+(\text{sol})_n}^0 - G_{Li^+}^0 - nG_{\text{sol}}$  is the solvation energy of Li<sup>+</sup>,  $D_{LiO_2^{\cdot}} = (G_{LiO_2^{\cdot}}^0 - G_{Li^+}^0 - G_{O_2^{\cdot-}}^0)$  is the strength of the Li – O bond in LiO<sub>2</sub>,  $c_{Li^+}$  and  $c_{Li^+}^{\text{ref}}$  are the local and reference lithium concentration, respectively.

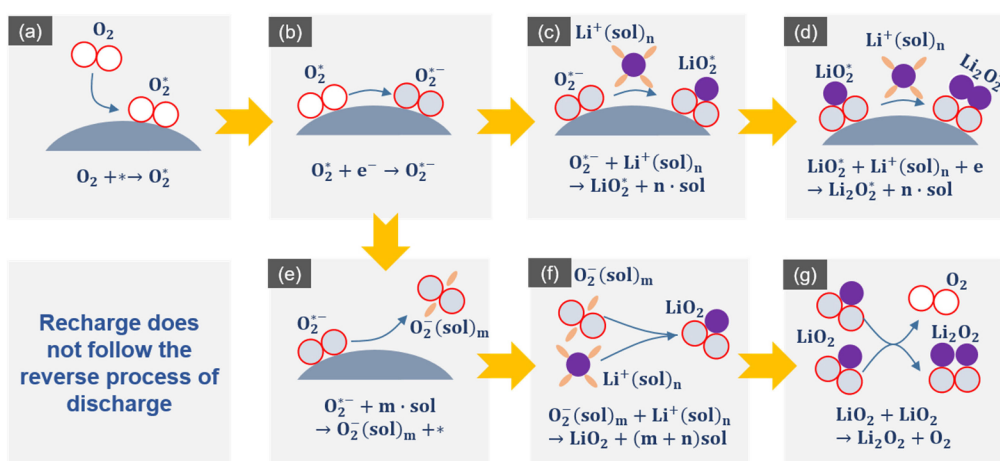


Figure 5. ORR mechanism during discharge.

An immediate corollary of Eq.(4) and (5) is that  $\text{LiO}_2^*$  formation is less favored in presence of strongly solvated  $\text{Li}^+$ , on the contrary,  $\text{O}_2^-(\text{sol})_m^*$  formation is more favored in presence of strongly solvated  $\text{O}_2^-$ .<sup>[31]</sup> The solvation energies of  $\text{Li}^+$  and  $\text{O}_2^-$  are related to the donor number (DN) of electrolyte solvent. As a result, the DN is good descriptor of the discharge mechanism. Specifically, in high DN solvent such as DMSO, the solvation of  $\text{Li}^+$  and  $\text{O}_2^-$  are strong, namely  $\Delta G_{\text{Li}^+}^{\text{sol}}$  and  $\Delta G_{\text{O}_2^-}^{\text{sol}}$  are more negative, therefore, the pathway involving  $\text{O}_2^-(\text{sol})_m^*$ , so-called solution mediated pathway, is more favored, while the pathway involving  $\text{LiO}_2^*$ , so-called surface mediated pathway, is less favored.<sup>[30b,c]</sup>

The potential dependence of the discharge mechanism has been revealed by Zhang et al.<sup>[30e]</sup> Lowering  $\phi^M$  not only promotes formation  $\text{O}_2^-$ , as seen from Eq.(3), but also facilitates the last step of the surface mediated pathway,  $\text{LiO}_2^* + \text{Li}^+(\text{sol})_n + e \rightarrow \text{Li}_2\text{O}_2 + ^* + n \bullet \text{sol}$ , thereby, lowering  $\theta_{\text{LiO}_2^*}$  and shifting  $\Delta G_{\text{LiO}_2^*}$  towards more negative values. This reasoning explains why the surface mediated pathway is more favored at lower potentials (larger overpotentials, and higher discharge current densities).

The thermodynamic analysis utterly neglects kinetic factors, which are essential for a complete understanding of reaction mechanisms of lithium-oxygen batteries. However, such unified thermodynamic-kinetic consideration for reactions in lithium-oxygen batteries is rare. In future, the theoretical framework developed for aqueous ORR on platinum electrodes may fill in this gap.<sup>[32]</sup> Although the pillars of the discharge mechanism have been established, there are still elusive issues, including but not limited to, does the reaction belong to the inner-sphere or outer-sphere type? What are the coordinate numbers of solvated  $\text{Li}^+$  and  $\text{O}_2^-$ ? How does the double layer impact the reaction? How does the porous structure of the  $\text{Li}_2\text{O}_2$  film impact the reaction? As aforementioned in the preceding section, some researchers contended that the ORR occurs on the electrode- $\text{Li}_2\text{O}_2$  interface.<sup>[27]</sup> If this is the case, one may be encountered with difficulties in understanding how the solution properties dictate the reaction pathway, as well-established in many studies.

Recharge mechanism of lithium-oxygen batteries is an ongoing challenge; there is no widely-accepted scheme for the present. Before going into the controversy on the mechanism, let us recapitulate major experimental phenomena that are confirmed by multiple sources and well-accepted now in this field. These experimental clues are the beacon guiding us along the way towards the correct mechanism. They are: (1) Viswanathan et al. measured the fundamental kinetic overpotential for OER in lithium-oxygen batteries and found that it is surprisingly small, i.e.,  $< 0.2$  V under a practical current density (10 mA/cm<sup>2</sup> with respect to the geometrical surface area);<sup>[29]</sup> (2) McCloskey et al. observed oxygen release at potentials below 3 V (vs Li/Li<sup>+</sup>) during recharge, and calculated the electron-oxygen ratio  $e/\text{O}_2$  being close to 2 at charging potentials below 4.0 V (vs Li/Li<sup>+</sup>) using DEMS;<sup>[26]</sup> (3) Ganapathy et al. identified an off-stoichiometric  $\text{Li}_{2-x}\text{O}_2$  compound using operando X-ray diffraction;<sup>[33]</sup> (4) Peng et al. did not find any

signal of  $\text{LiO}_2$  in a SERS study carried on a lithium-oxygen cell with Au as the electrode and low DN acetonitrile (ACN) as the solvent;<sup>[30a]</sup> (5) Wandt et al.<sup>[34]</sup> and Mahne et al.<sup>[35]</sup> probed formation of singlet oxygen  ${}^1\text{O}_2$  since the onset of recharge.

In addition to the experimental route, the theoretical route also provides very insightful findings. An early DFT study by Hummelshøj et al. reported that the thermodynamic overpotential (namely the potential above which the multi-step reaction pathway descends along the reaction coordinate) of oxidation of  $\text{Li}_2\text{O}_2$  can be lower than 0.2 V.<sup>[36]</sup> Later on, Kang et al. proposed a facile mechanism for oxidation of  $\text{Li}_2\text{O}_2$  involving the off-stoichiometric  $\text{Li}_{2-x}\text{O}_2$ , and it was further pointed out the lowest energy  $\text{Li}_{2-x}\text{O}_2$  is a composite of  $\text{LiO}_2$  and  $\text{Li}_2\text{O}_2$  domains.<sup>[37]</sup>

Concerted experimental and theoretical efforts discussed above reveal several key points of the OER in lithium-oxygen batteries, while a self-consistent mechanistic picture interlinking these points is missing yet.

A very recent study from Lu et al. provides a flexible scheme unifying different viewpoints reported before.<sup>[38]</sup> In this scheme, the OER begins with topotactic delithiation of  $\text{Li}_2\text{O}_2$  forming  $\text{Li}_{2-x}\text{O}_2$ , which either generates soluble  $\text{LiO}_2$  in electrolytes with a high DN solvent such as DMSO,  $\text{Li}_{2-x}\text{O}_2 \rightarrow \text{LiO}_{2(\text{sol})} + (1-x)\text{Li}^+ + (1-x)e$ , or undergoes an electrochemical reaction releasing  $\text{O}_2$ ,  $\text{Li}_{2-x}\text{O}_2 \rightarrow \text{O}_2 + (2-x)\text{Li}^+ + (2-x)e$ . In the former route, soluble  $\text{LiO}_2$  undergoes disproportionation,  $\text{LiO}_{2(\text{sol})} + \text{LiO}_{2(\text{sol})} \rightarrow \text{Li}_2\text{O}_2 + \text{O}_2$ . It is speculated that a considerable amount of  $\text{O}_2$  may be in the singlet state, triggering parasitic reactions degrading the cycling performance.

Evidences for the soluble  $\text{LiO}_2$ , the pillar of this appealing scheme, are twofold: the ring current observed above 3.7 V (vs Li/Li<sup>+</sup>) in the thin-film rotating ring-disk electrode (RRDE) experiment, and the adsorption peak at 529.4 eV in O K-edge XANES characterization conducted on chemically-synthesized  $\text{Li}_2\text{O}_2$ . Most impressive is the contrast that the above phenomena observed in a high DN solvent are absent in a low DN solvent.

Inspired by morphological and electrochemical evidences discussed above, we speculate a mechanistic scheme for recharge, as depicted in Figure 6. In this scheme, the intrinsic

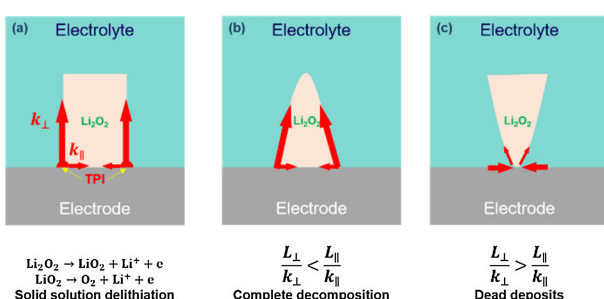


Figure 6. Schematic illustration of  $\text{Li}_2\text{O}_2$  decomposition during recharge.

decomposition of  $\text{Li}_2\text{O}_2$  follows a reversible pathway of formation of  $\text{Li}_2\text{O}_2$ , which is feasible as DFT calculations and

electrochemical measurements reveal that the fundamental kinetic overpotential of  $\text{Li}_2\text{O}_2$  oxidation is small relative to aqueous OER.<sup>[29,36]</sup> The reaction site is at the triple-boundary interface between the electrode,  $\text{Li}_2\text{O}_2$  and the electrolyte. Topotactic delithiation of  $\text{Li}_2\text{O}_2$  generates  $\text{LiO}_2$ , which together with  $\text{Li}_2\text{O}_2$  form the  $\text{Li}_{2-x}\text{O}_2$  phase. Probably, a fraction of  $\text{LiO}_2$  dissolves into the electrolyte and undergoes disproportionation. The  $\text{Li}_{2-x}\text{O}_2$  phase has a higher electronic conductivity than the  $\text{Li}_2\text{O}_2$  phase, therefore, paving a conducting path on the  $\text{Li}_2\text{O}_2$  surface. As a result, decomposition of  $\text{Li}_2\text{O}_2$  proceeds in two directions: the direction along the interface between  $\text{Li}_2\text{O}_2$  and the electrode, and the direction along the  $\text{Li}_2\text{O}_2$  surface. The decomposition rates in these two directions are denoted as  $k_{\parallel}$  and  $k_{\perp}$ , respectively. The characteristic length of  $\text{Li}_2\text{O}_2$  in these two directions are denoted as  $L_{\parallel}$  and  $L_{\perp}$ , respectively. As a crude approximation, two scenarios can be envisioned. If  $L_{\parallel}/k_{\parallel} > L_{\perp}/k_{\perp}$ ,  $\text{Li}_2\text{O}_2$  decomposition proceeds with a pyramid shape, as portrayed in Figure 6 (b), and the benign contact between the electrode and  $\text{Li}_2\text{O}_2$  will be retained until complete decomposition. Otherwise,  $\text{Li}_2\text{O}_2$  decomposition proceeds with an inverted pyramid shape, as portrayed in Figure 6 (c), and at a certain stage  $\text{Li}_2\text{O}_2$  will be disconnected from the electrode, resulting in dead deposits of  $\text{Li}_2\text{O}_2$  that cannot be decomposed further. In this case, further recharge will incur electrolyte decomposition, accompanied with an ascending voltage curve frequently seen in the later stage of recharge. Following this line of reasoning, the key to ensuring a complete decomposition of  $\text{Li}_2\text{O}_2$  and avoiding electrolyte decomposition is to maintain  $L_{\parallel}/k_{\parallel} > L_{\perp}/k_{\perp}$ . This relation can be satisfied when  $L_{\parallel} \gg L_{\perp}$ , namely film-like  $\text{Li}_2\text{O}_2$  or when  $k_{\parallel} \ll k_{\perp}$ , namely heterogeneous decomposition rate.

## 5. Concluding Remarks

Considerable amount of knowledge on fundamental issues of lithium-oxygen batteries has been generated from active research in the past decade. We are now standing on the brink of unifying relevant knowledge into a self-consistent mechanistic picture.

On charge transport across the  $\text{Li}_2\text{O}_2$  thin film, two mechanisms, namely hole-tunneling and hole-polarons migration, have been proposed; they are successful in explaining a certain regime of discharge, but faced with difficulties in explaining the whole process. The fact that the  $\text{Li}_2\text{O}_2$  film is ultra-thin renders that nonlinearities and double layer effects should not be neglected. In addition, as the concentration of charge carrier is strongly spatial-dependent, we argue that a single-valued conductivity is insufficient to describe the charge transport properties. Moreover, previous works on this topic usually assume that the  $\text{Li}_2\text{O}_2$  film is compact and homogenous. Future efforts should also be based on the fact that the  $\text{Li}_2\text{O}_2$  film could be porous and heterogeneous.

On the reaction sites, the current status of reaction sites reminds us of the parable of the blind and the elephant, each one holds his own opinion based on which part he feels of the elephant with a specific tool in hand. The situation here is even

more complex, as the elephant touched by different blind men may be different. It then comes no surprise that there is heated debate on the location of the reaction site. Nevertheless, there is growing consensus that reaction sites during discharge and charge are asymmetrical. Specifically, ORR occurs on the  $\text{Li}_2\text{O}_2$ -electrolyte interface during discharge, while OER occurs on the electrode- $\text{Li}_2\text{O}_2$  interface during recharge. In future, multiple *in-situ*, cross-validated methods should be combined to achieve a comprehensive understanding.

On the reaction mechanism, we have already obtained a well-knitted mechanistic scheme for the discharge reaction, while the charge reaction mechanisms remain elusive and controversial. A simple thermodynamic analysis is able to understand how the electrolyte properties, the electrode potential, and the electrode surface properties dictate the discharge reaction. There have been initial efforts to propose a unifying mechanistic scheme for the charge reaction. However, it awaits more evidences, especially those on the reaction intermediate. In future, unified thermodynamic-kinetic considerations should be imposed on oxygen reactions in lithium-oxygen batteries.

We would like to close this review paper by revisiting the article entitled "the method of multiple working hypotheses" written in 1890 by Chamberlin.<sup>[39]</sup> In this article, Chamberlin criticized the process: "a premature explanation passes into a tentative theory, then into an adopted theory, and then into a ruling theory", due to "an unconscious selection and magnifying of the phenomena that fall into harmony with the theory and support it, and an unconscious neglect of those that fail of coincidence." Unfortunately, this research paradigm of "ruling theories" does not pass away even after more than one century and lingers to the present day in many fields including that of lithium-oxygen batteries reviewed here. The research method of "multiple working hypotheses", of which the essence is to embrace every rational explanation of the phenomena, and to develop every possible hypotheses without "partility of intellectual parentage", is yet to play a dominant role. Nevertheless, we deem that the method of "multiple working hypotheses" is key to clarifying controversies discussed in this review in future.

## Acknowledgements

J. Huang appreciates financial support from Central South University (no. 502045001). Z.P. is indebted to the National Natural Science Foundation of China (no. 91545129, 21575135, 21733012, 21633008 and 21605136), the "Strategic Priority Research Program" of the CAS (no. XDA09010401) and the Ministry of Science and Technology of China (no. 2016YBF0100100).

## Conflict of Interest

The authors declare no conflict of interest.

**Keywords:** charge transport • lithium-oxygen batteries • oxygen evolution reaction • oxygen reduction reaction • reaction interfaces

- [1] G. E. Blomgren, *J. Electrochem. Soc.* **2017**, *164*, A5019-A5025.
- [2] a) E. Peled, S. Menkin, *J. Electrochem. Soc.* **2017**, *164*, A1703-A1719; b) M. Winter, in *Z. Phys. Chem. (Muenchen Ger.)*, **2009**, *223*, 1395–1406.
- [3] P. Lu, S. J. Harris, *Electrochem. Commun.* **2011**, *13*, 1035–1037.
- [4] V. Viswanathan, K. S. Thygesen, J. S. Hummelshøj, J. K. Nørskov, G. Girishkumar, B. D. McCloskey, A. C. Luntz, *J. Chem. Phys.* **2011**, *135*, 214704.
- [5] Z. Ogumi, *Electrochemistry* **2010**, *78*, 319–324.
- [6] P. Albertus, G. Girishkumar, B. McCloskey, R. S. Sánchez-Carrera, B. Kozinsky, J. Christensen, A. C. Luntz, *J. Electrochem. Soc.* **2011**, *158*, A343-A351.
- [7] a) M. D. Radin, D. J. Siegel, *Energy Environ. Sci.* **2013**, *6*, 2370–2379; b) F. Tian, M. D. Radin, D. J. Siegel, *Chem. Mater.* **2014**, *26*, 2952–2959; c) J. B. Varley, V. Viswanathan, J. K. Nørskov, A. C. Luntz, *Energy Environ. Sci.* **2014**, *7*, 720–727; d) M. D. Radin, C. W. Monroe, D. J. Siegel, *J. Phys. Chem. Lett.* **2015**, *6*, 3017–3022; e) S. P. Ong, Y. Mo, G. Ceder, *Phys. Rev. B* **2012**, *85*, 081105.
- [8] A. C. Luntz, V. Viswanathan, J. Voss, J. B. Varley, J. K. Nørskov, R. Scheffler, A. Speidel, *J. Phys. Chem. Lett.* **2013**, *4*, 3494–3499.
- [9] K. B. Knudsen, A. C. Luntz, S. H. Jensen, T. Vegge, J. Hjelm, *J. Phys. Chem. C* **2015**, *119*, 28292–28299.
- [10] J. G. Simmons, *J. Appl. Phys.* **1963**, *34*, 1793–1803.
- [11] A. C. Luntz, B. D. McCloskey, *Chem. Rev.* **2014**, *114*, 11721–11750.
- [12] B. D. Adams, C. Radtke, R. Black, M. L. Trudeau, K. Zaghib, L. F. Nazar, *Energy Environ. Sci.* **2013**, *6*, 1772–1778.
- [13] J. Huang, B. Tong, Z. Li, T. Zhou, J. Zhang, Z. Peng, *J. Phys. Chem. Lett.* **2018**, *9*, 3403–3408.
- [14] J. Liu, S. Khaleghi Rahimian, C. W. Monroe, *Phys. Chem. Chem. Phys.* **2016**, *18*, 22840–22851.
- [15] T. Vegge, J. M. Garcia-Lastra, D. J. Siegel, *Curr. Opin. Electrochem.* **2017**, *6*, 100–107.
- [16] a) O. Gerbig, R. Merkle, J. Maier, *Adv. Mater.* **2013**, *25*, 3129–3133; b) Y. Zhang, Q. Cui, X. Zhang, C. McKee William, Y. Xu, S. Ling, H. Li, G. Zhong, Y. Yang, Z. Peng, *Angew. Chem. Int. Ed.* **2016**, *55*, 10717–10721; *Angew. Chem.* **2016**, *128*, 10875–10879.
- [17] a) J. Jamnik, J. Maier, *J. Electrochem. Soc.* **1999**, *146*, 4183–4188; b) J. Jamnik, J. Maier, S. Pejovnik, *Electrochim. Acta* **1999**, *44*, 4139–4145; c) J. Jamnik, J. Maier, *Phys. Chem. Chem. Phys.* **2001**, *3*, 1668–1678.
- [18] W. Lai, S. M. Haile, *J. Am. Ceram. Soc.* **2005**, *88*, 2979–2997.
- [19] N. Kaiser, S. Bradler, C. König, B. Roling, *J. Electrochem. Soc.* **2017**, *164*, A744-A749.
- [20] L. Zhong, R. R. Mitchell, Y. Liu, B. M. Gallant, C. V. Thompson, J. Y. Huang, S. X. Mao, Y. Shao-Horn, *Nano Lett.* **2013**, *13*, 2209–2214.
- [21] H. Zheng, D. Xiao, X. Li, Y. Liu, Y. Wu, J. Wang, K. Jiang, C. Chen, L. Gu, X. Wei, Y.-S. Hu, Q. Chen, H. Li, *Nano Lett.* **2014**, *14*, 4245–4249.
- [22] H.-D. Lim, B. Lee, Y. Bae, H. Park, Y. Ko, H. Kim, J. Kim, K. Kang, *Chem. Soc. Rev.* **2017**, *46*, 2873–2888.
- [23] A. Kushima, T. Koido, Y. Fujiwara, N. Kuriyama, N. Kusumi, J. Li, *Nano Lett.* **2015**, *15*, 8260–8265.
- [24] P. Liu, J. Han, X. Guo, Y. Ito, C. Yang, S. Ning, T. Fujita, A. Hirata, M. Chen, *Sci. Rep.* **2018**, *8*, 3134.
- [25] K. He, X. Bi, Y. Yuan, T. Foroozan, B. Song, K. Amine, J. Lu, R. Shahbazian-Yassar, *Nano Energy* **2018**, *49*, 338–345.
- [26] B. D. McCloskey, R. Scheffler, A. Speidel, G. Girishkumar, A. C. Luntz, *J. Phys. Chem. C* **2012**, *116*, 23897–23905.
- [27] J. Wang, Y. Zhang, L. Guo, E. Wang, Z. Peng, *Angew. Chem. Int. Ed.* **2016**, *55*, 5201–5205; *Angew. Chem.* **2016**, *128*, 5287–5291.
- [28] J. Huang, B. Tong, *Chem. Commun.* **2017**, *53*, 11418–11421.
- [29] V. Viswanathan, J. K. Nørskov, A. Speidel, R. Scheffler, S. Gowda, A. C. Luntz, *J. Phys. Chem. Lett.* **2013**, *4*, 556–560.
- [30] a) Z. Peng, S. A. Freunberger, L. J. Hardwick, Y. Chen, V. Giordani, F. Bardé, P. Novák, D. Graham, J.-M. Tarascon, P. G. Bruce, *Angew. Chem. Int. Ed.* **2011**, *50*, 6351–6355; *Angew. Chem.* **2011**, *123*, 6475–6479; b) L. Johnson, C. Li, Z. Liu, Y. Chen, S. A. Freunberger, P. C. Ashok, B. B. Praveen, K. Dholakia, J.-M. Tarascon, P. G. Bruce, *Nat. Chem.* **2014**, *6*, 1091–1099; c) N. B. Aetukuri, B. D. McCloskey, J. M. García, L. E. Krupp, V. Viswanathan, A. C. Luntz, *Nat. Chem.* **2015**, *7*, 50–56; d) X. Gao, Y. Chen, L. Johnson, P. G. Bruce, *Nat. Mater.* **2016**, *15*, 882–888; e) Y. Zhang, X. Zhang, J. Wang, W. C. McKee, Y. Xu, Z. Peng, *J. Phys. Chem. C* **2016**, *120*, 3690–3698.
- [31] a) D. G. Kwabi, V. S. Bryantsev, T. P. Batcho, D. M. Itkis, C. V. Thompson, Y. Shao-Horn, *Angew. Chem. Int. Ed.* **2016**, *55*, 3129–3134; *Angew. Chem.* **2016**, *128*, 3181–3186; b) C. O. Laoire, S. Mukerjee, K. M. Abraham, E. J. Plichta, M. A. Hendrickson, *J. Phys. Chem. C* **2010**, *114*, 9178–9186.
- [32] J. Huang, J. Zhang, M. Eikerling, *Phys. Chem. Chem. Phys.* **2018**, *20*, 11776–11786.
- [33] S. Ganapathy, B. D. Adams, G. Stenou, M. S. Anastasaki, K. Goubitz, X.-F. Miao, L. F. Nazar, M. Wagemaker, *J. Am. Chem. Soc.* **2014**, *136*, 16335–16344.
- [34] J. Wandt, P. Jakes, J. Granwehr, H. A. Gasteiger, R.-A. Eichel, *Angew. Chem.* **2016**, *128*, 7006–7009; *Angew. Chem. Int. Ed.* **2016**, *55*, 6892–6895.
- [35] N. Mahne, B. Schafzahl, C. Leybold, M. Leybold, S. Grumm, A. Leitgeb, Gernot A. Strohmeier, M. Wilkening, O. Fontaine, D. Kramer, C. Slugovc, Sergey M. Borisov, Stefan A. Freunberger, *Nat. Energy* **2017**, *2*, 17036.
- [36] J. S. Hummelshøj, J. Blomqvist, S. Datta, T. Vegge, J. Rossmeisl, K. S. Thygesen, A. C. Luntz, K. W. Jacobsen, J. K. Nørskov, *J. Chem. Phys.* **2010**, *132*, 071101.
- [37] S. Kang, Y. Mo, S. P. Ong, G. Ceder, *Chem. Mater.* **2013**, *25*, 3328–3336.
- [38] Y. Wang, N.-C. Lai, Y.-R. Lu, Y. Zhou, C.-L. Dong, Y.-C. Lu, *Joule* **2018**.
- [39] T. C. Chamberlin, *Science* **1965**, *148*, 754–759.

Manuscript received: August 22, 2018

Accepted Article published: October 9, 2018

Version of record online: October 31, 2018